RSC Advances

RSC Advances

ARTICLE

Green synthesis of ZnO hollow sphere nanostructures by facile route at room temperature with efficient photocatalytic dye degradation

Seyed Mohsen Mousavi, Ali Reza Mahjoub,* and Reza Abazari

The present work has prepared ZnO hollow spherical nanoparticles using a straightforward synthetic route and has innovatively made use of the carbon sphere as template at room temperature. Through powder X-ray diffraction (PXRD), field-emission scanning electron microscopy (FE-SEM), and fourier transform infra-red spectroscopy (FT-IR) the obtained hollow spheres were characterized. Also, the hollow structure is demonstrated by the different brightness in the High-resolution transmission electron microscopy (HRTEM) images. These hollow spheres were approximately 1 µm in diameter and were walled with some ZnO aggregate nanoparticles with dimensions of approximately 55 nm. In order to degrade the congo red dye (CR dye), the said ZnO nanostructures were then adopted as photo-catalyst. Based on the results, under both UV and visible radiations, the prepared ZnO hollow spherical nanocrystallines outperformed other zinc oxide morphologies in terms of CR dye photodegradation, which can be ascribed to the more appropriate photocatalytic characteristics of the suggested particles. Finally, the possible mechanism for growth has been fully explained.

Introduction

Nowadays, a major well known environmental concern is aquatic systems contamination caused by different organic pollutants as a result of the human population growth and the extensive development of industry [1]. A green ecological method to remove or harmful pollutants organic compounds is photocatalysis, which was widely investigated for resolving environmental issues [2]. Various semiconductors, such as ZnO [3], TiO_2 [4], CuO [5], NiO [6], WO_3 [7], $BiVO_4$ [8], and $LaPO_4$ [9] have been utilized as photocatalyst to remove inorganic or organic pollutants in harmful waste with the photodegradation. Due to their inclusion of large band gap, harmless nature, and high photosensitivity, ZnO and TiO_2 have been assumed to be the superior photocatalytic materials among the said photocatalysts [10, 11]. In comparison with TiO_2, ZnO as a multipurpose material belongs to a direct n-type semiconductor with a broad bandgap of 3.2 eV near to TiO_2, and it has benefits containing high thermal and chemical stability, high electrochemical coupling factor, high photostability, high catalytic activity, appropriate bandgap, cost effectiveness and eco-friendly. [12]. Moreover, various studies have reported ZnO as a promising photocatalyst because its photocatalytic peformace and the quantum performance are higher compared with TiO_2 [13]. Furthermore, zinc oxide, with its unique chemical and physical features, can absorb a larger portion of the solar spectrum compared with TiO_2, and so ZnO photocatalyst is recognized more appropriate for photocatalytic

degradation in the exposure of sunlight [14].

Based on literature, it should be noted that specific surface area, morphologies and particles size effectively impact on the photocatalytic activity of ZnO [15]. In recent years, well-defined ZnO nanostructures with different morphologies including nanowire, nanorods, nanotubes, nanoflowers and nanosphere were reported. Much attention has been paid to Zinc oxide hollow structures as a unique class of structured materials due to their structural benefits that offer singular chemical and physical characteristics [16]. Since hollow spheres show high surface area, low density, distinct optical properties, and good permeation [17], they have attracted great attention among the researchers and have thus been widely used in preparation of the functional materials due to their applicability in numerous fields such as the low dielectric constant materials, fillers, catalysts, pigments, protection of light-sensitive components, and chemical storage. Preparation of the porous or hollow ZnO structures has already been carried out using several different approaches. Yang et al. introduced a protocol for synthesis of two hollow ZnO structures using sulfonated polystyrene (PS) microspheres as template, and thus they removed the PS cores through the solvent extraction or calcination [18]. In a study conducted by Bai et al., using a copolymer controlled self-assembly method, clew-like ZnO superstructures were provided in urea presence [19]. Jiang et al. prepared ZnO hollow spheres using ethanol droplets as soft templates [20]. However, in the said methods, heterogeneous product sizes were obtained and the experimentations were too complex. Therefore, developing a simple synthesis method with mild conditions (e.g., low temperatures and reduced workup) is highly desired. The template-based preparation route is shown to be the most efficient and multifunctional strategy for generation of

Department of Chemistry, Tarbiat Modares University, Tehran, Iran. E-mail: mahjouba@modares.ac.ir; smm4566@gmail.com; reza.abazari@modares.ac.ir; Fax: +98 21 82883455; Tel.: +98 21 82883442.

inorganic hollow superstructures. For the synthesis of the hollow spherical materials, different hard and soft templates have already been applied. Examples of hard templates are polystyrene spheres, gas-bubbles, polymer microspheres, and silicon spheres, while the soft ones involve supramolecular, ionic liquids, surfactants, and organogels. As an example, hollow ZnO microspheres have already been synthesized templated by ultrasound irradiation combined with carbon spheres [21].

The present study has introduced a straightforward, green, and energy-efficient route for preparation of the ZnO hollow spherical nanostructures using carbon microspheres as template in the absence of the ultrasound generator, while the need for application of the complex tools and catalytic metals has been removed. Besides, CR dye degradation has been considered to examine the photocatalytic activity of these hollow spheres. To the best of our knowledge, no report has previously been given on the photocatalytic activity of ZnO with hollow sphere morphology for congo red degradation.

Experimental details

Materials and physical techniques

All reagents for the synthesis and analysis were commercially available from Merck Company and used as received. Doubly-distilled water was used to prepare aqueous solutions. The infrared spectra were recorded on a nicolet fourier transform IR, nicolet 100 spectrometer in the range 500-4000 cm^{-1} using the KBr disk technique. Powder X-ray diffraction (PXRD) measurements were performed using a Philips X'pert diffractometer with monochromated Cu-K_α radiation (λ= 1.54056 Å). Also, the morphology of samples was characterized by a field emission scanning electron microscope (FE-SEM) (Mira TESCAN) with gold coating. The UV-Vis absorption spectra were examined on a UV-Visible spectrometer (Shimadzu UV 2100). High-resolution transmission electron microscopy (HRTEM) images were recorded with a Philips cm 30 instrument.

Preparation of carbon microspheres

Carbon microspheres were prepared according to a reported procedure [22] with some modifications. A clear solution (~ 0.5 mol/L) containing 8.7 g of fructose and 100 mL of water was placed in a 150 mL of teflon-lined stainless steel autoclave and maintained at 180 ℃ for 4 h. Then, the solution was cooled to room temperature. The pure products were collected by centrifugation and washed several time with distilled water and ethanol, then dried at 80 ℃ in an oven overnight.

Preparation of Zinc Oxide hollow spherical nanostructures

In a typical synthesis, 2.2 g of zinc(II) acetate dihydrate in 40 ml of distilled water and 1 g of carbon microspheres were uniformly dispersed in 20 ml of distilled water as templates were added in stirring bath at room temperature for 5 h. Then, the mixed solution was aged under ambient conditions for one day. The product was centrifuged and washed with distilled water, and were annealed from room temperature to 500 °C at a rate of 1℃ min^{-1}, and then held at 500 °C for 2 h in air. ZnO hollow spheres with a white color were finally obtained. Finally, the photocatalytic activity for degradation of CR dye was studied.

Photocatalytic reaction studies

The photocatalytic performance of ZnO hollow spheres was evaluated in the photodegradation reaction of CR dye under UV and visible light. To study the photocatalytic reaction, 50 ml of the 20 ppm solution of CR (as a anionic dye) was used as a suspension

along with 25 mg of the catalyst in an open Pyrex reaction vessel and irradiated using UV lamp (30 W, UV-C = 253.7 nm). The suspension was magnetically stirred during the photolysis. Air was blown in to the reaction by an air pump to maintain the solution saturated with oxygen during the reaction. During photocatalytic reaction, the temperature of the dispersions was maintained at 25 ℃. Firstly, dye solution was stirred in the dark for 30 min. Then, the suspension was irradiate by UV and visible lamp and three milliliters of the homogenized dispersion aliquots were taken at regular intervals, starting from zero time and centrifuged at 4000 rpm for 5 min. The reaction was monitored as a function of illumination time by measuring the absorbance of CR dye.

Results and discussion

Analysis of ZnO hollow spheres

Great importance is attached to the investigation of the aggregation state, size, shape, and morphology of the nano-materials. The structure, morphology, and size distribution of the nanostructures are influenced by the corresponding preparation conditions [23, 24]. Numerous studies have already been conducted on the different growth factors that influence the morphological and electro-optic characteristics of ZnO materials. However, scant attention has been paid to the investigation of the morphology and photo-catalytic applications of ZnO. Based on such mono-factor studies, the photo-catalytic characteristics of ZnO structures are affected by their preferred orientation, size and morphology. The present study has developed an eco-friendly hard template chemical route for preparation of the nanostructured ZnO hollow spheres. Our suggested approach produces no impurities and seems to be appropriate for modern chemical preparation. In this context, as shown in Fig. 1, using FE-SEM analysis, surface morphology of the prepared ZnO hollow spheres are first taken into account.

FE-SEM images of the as-prepared zinc oxide-carbon composite microspheres before calcination are shown in Figs. 1a and 1b. These spheres have smooth surfaces. Besides, they show an average diameter of 2-5 μm and are aggregated and interconnected. As shown in Fig. 1c, after calcination, a drastic decrease in the diameters of the said spheres is observed, an so the sizes of the spheres become about 1-2 μm. During calcination, some significant shrinkage (from about 4 to 1 μm in size) in the structure occurs, which represents the conversion of the loosely-adsorbed zinc ions on the carbon spheres into the network of the dense zinc oxides in the hollow spherical shells. Besides, as shown in Figs. 1c-h, the rough and porous surfaces of the said structures are indicative of the fact that the ZnO hollow spherical shells are made of a large number of small nanoparticles. Under the heating rate of 1 ℃ min^{-1} from room temperature to 500 °C, hollow spherical morphology and zinc oxide nanoparticles with dimensions of about 55 nm were obtained – as indicated by the FE-SEM images of the prepared samples (Figs. 1c, d). On the other hand, as shown in Figs. 1e-h, through the consideration of similar temperature but upper heating rates of 2 and 4 ℃ min^{-1}, calcination processes were conducted to investigate the heating rate effects on the shape and size of the ZnO hollow spherical structures. Consequently, the sizes and morphologies of these hollow spherical particles are influenced by the rate of the heating, which in turn leads to the provision of intact hollow spheres at 1 ℃ min^{-1} as the lowest rate of heating. As represented by Figs. 1e-h, as the heating rate increases to 2 and 4 ℃ min^{-1}, the ZnO hollow spheres are observed to be broken. The higher heating rate is likely to result in a too fast phase variation, which might in turn lead to the breakage of the materials.

Please do not adjust margins

RSC Advances

ARTICLE
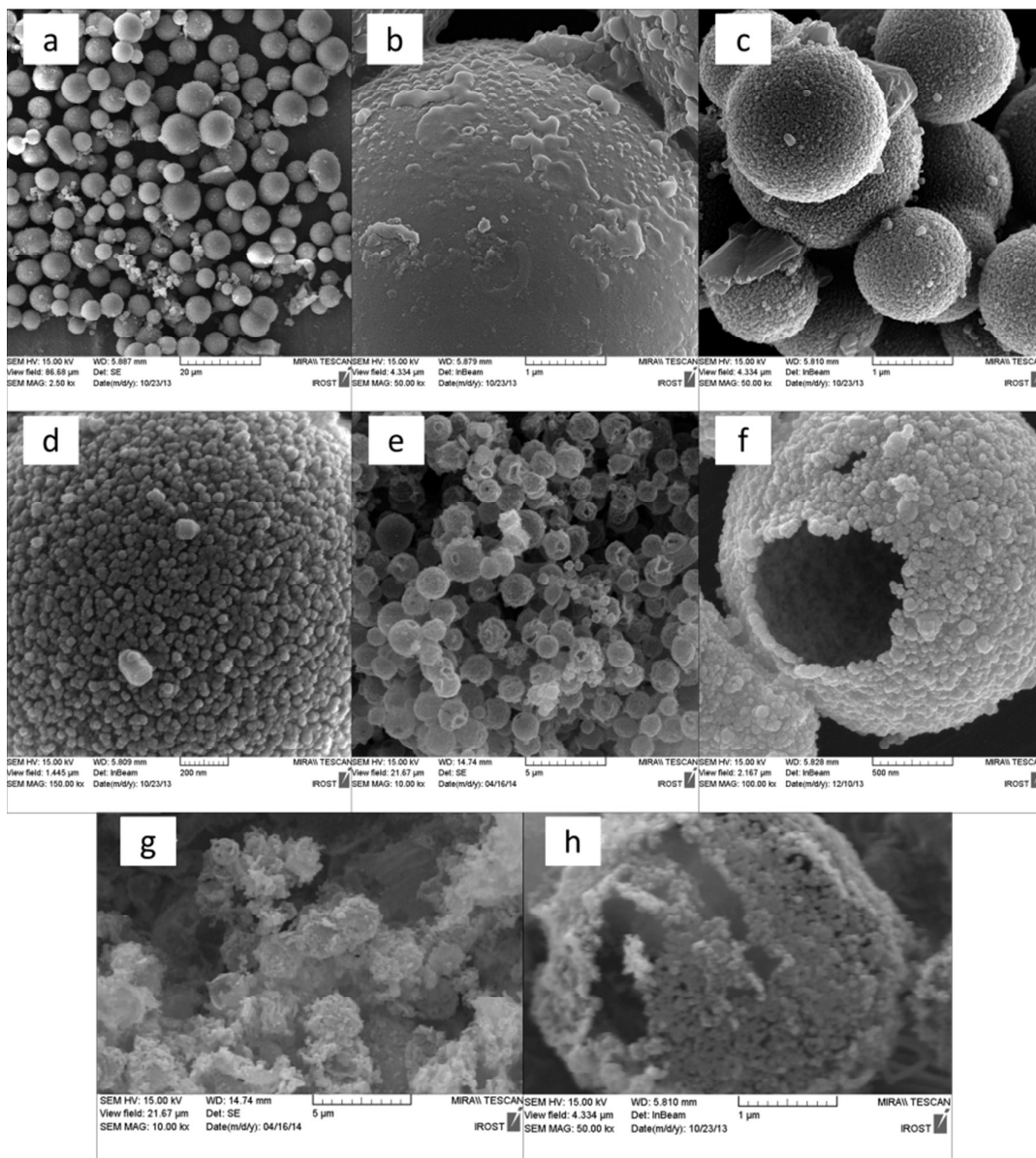
Fig. 1 FE-SEM images of carbon sphere@ZnO (core/shell) before calcination (a, b), the ZnO hollow spheres obtained by calcination at 500 ℃ at the heating rate of 1 ℃ min^{-1} (c, d), 2 ℃ min^{-1} (e, f), and 4 ℃ min^{-1} (g, h) in two different scale bars.

A brief review of the related literature demonstrates that, photocatalytic activity is in close relation with the photo-catalyst's BET surface area, as well as the size and shape of the particles [25, 26]. Accordingly, through measuring the N$_2$ adsorption-desorption, the Brunauer Emmett Teller (BET) specific surface area of ZnO hollow sphere prepared at 500 ℃ was then determined. Table 1 represents the physical parameters of the materials achieved through

the N$_2$ adsorption-desorption procedure. Using Brunauer-Emmett-Teller (BET) equation, a specific surface area of 14.6 m^{2}g^{-1} has been obtained for the prepared ZnO hollow sphere powder. Since the increased BET surface area is likely to increase the reactant adsorption, it can be generally assumed that the products with higher BET surface area have a higher photocatalytic activity. According to Table 1, the aforementioned results demonstrate the orders of the photocatalytic efficiency as follows: pure carbon sphere > ZnO hollow

spheres > Carbon sphere@ZnO > Bulk ZnO.

Table 1 Specific surface area (BET) and chemical analysis of as-synthesized products.

| Specimen	ZnO Bulk	Pure carbon sphere	Carbon sphere @ZnO	ZnO hollow spheres
BET (m^{2}g^{-1})	5	37	5.89	14.6

Based on our synthesis template for preparation of the pure carbon microspheres [22], using the hydrothermal method and at 180 ℃, fructose solution has been used for synthesis of the spherical carbonaceous solids. Figs. 2a and b shows the FE-SEM image of the surface of the prepared pure carbon microspheres under the hydrothermal conditions. As it is shown, the surfaces of the carbon microspheres are rough and granulated. The granules on the surfaces are approximately 5 nm in size, which is in a good agreement with the previous results in the literature [27]. More exactly, it can thus be suggested that the surfaces of the carbon spheres are formed through the aggregate of some homogenous carbonaceous particles with the sizes of 5 nm. Due to such small particle sizes, the surface area can be increased. As reported in Table 1, the surface area of the pure carbon spheres is about 37 m^{2}g^{-1}. When this surface is covered by the ZnO precursors, the surface area is reduced to such an extent that the carbon sphere@ZnO before the calcination of the surface area, for example, decreases to 5.89 m^{2}g^{-1}. When carbon sphere@ZnO is calcined, it changes into the ZnO hollow spheres, which have a larger surface area (i.e., 14.6 m^{2}g^{-1}) than the carbon sphere@ZnO due to the formation of the vacant space in their centre. However, since the ZnO particles formed on the surface have a size of about 55 nm, they naturally have a smaller surface area than the pure carbon microspheres (Fig. 2c).
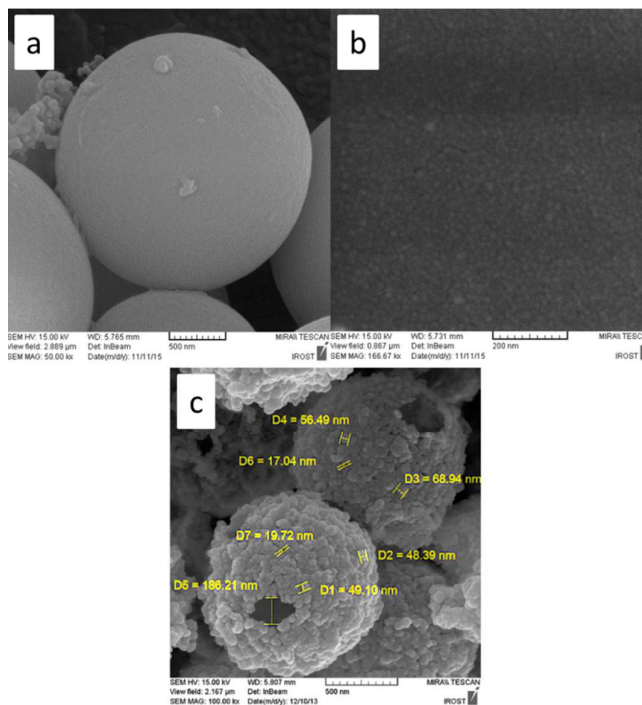
Fig. 2 FE-SEM images of pure carbon spheres (a, b) in two different scale bars and the ZnO hollow spheres obtained by calcination at 500 ℃ (c).

Moreover, HRTEM analysis has been employed for further justification and understanding of the hollow structure and composition of the final product. Fig. 3 shows the HRTEM analysis of the ZnO hollow spheres calcined at 500 ℃ at the heating rate of 1 ℃ min^{-1} as the best photocatalytic material in the present study. Based on the aforesaid figure, the products have hollow spherical microstructures. This can be accounted for by the fact that, in the images, a light inner part and a relatively darker outer spherical part exist, and thus the spheres are made of two layers. To put it differently, there is a marked contrast between the dark edges and bright centers in the HRTEM images, which is representative of the hollow structure of the ZnO hollow spheres. This finding is in agreement with the results of the FE-SEM analysis. Beside, an appropriate overlap between these parts can be observed with good transparency. This figure also shows that the synthesized ZnO hollow spheres are from 1 µm to 1.5 µm in diameter, whereas the coarse shell is calculated to have a thickness of around 55 nm.
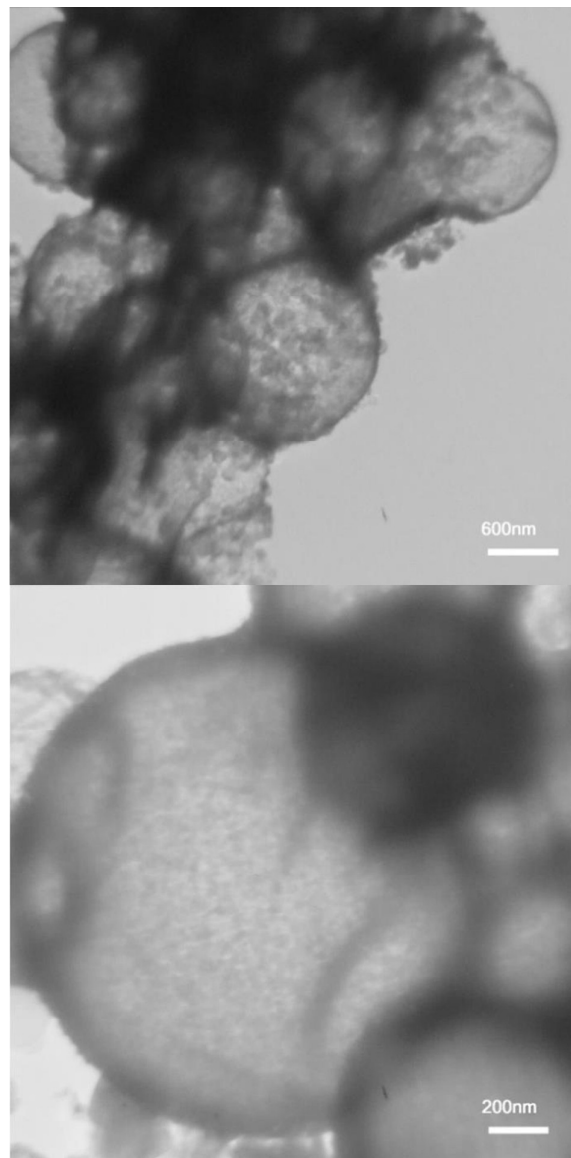

Fig. 3 HR-TEM images of the ZnO hollow spheres obtained by calcination at 500 ℃ at the heating rate of 1 ℃ min^{-1}; in two different scale bars.

Besides, the variations in the phase structure and crystallite size of the as-prepared ZnO powders before and after calcination have been

investigated using PXRD images. As shown in Fig. 4a, before calcination, the as-prepared composite microspheres are amorphous in the presence of fructose. Moreover, the X-ray diffraction pattern of zinc oxide hollow spheres after calcination is represented by Fig. 4b. The figure shows that the phase structure changes due to the increase in the calcination temperature to 500 ℃. Also, during calcination, crystallinity is seen to increase. With the lattice constants a = 3.249 Å and c = 5.207 Å (JCPDS card 36-1451), all the diffraction peaks are properly indexed to the wurtzite hexagonal ZnO. With respect to the prepared sample, diffraction peaks at 2θ values matching with 100, 002, 101,102, 110, 103, 200, 112, 001 and 202 planes of orthorhombic AIS phase were observed. Due to the complete removal of the carbon microsphere templates, no other diffraction peaks are observable in the pattern.

FT-IR spectra of the zinc oxide hollow sphere nanostructures are shown in Fig. 4c. In the region 800-900 cm^{-1} flexural vibration of OH, the off-screen absorption bands were observed. The existence of Zn-O stretching vibrational modes can be understood from the presence of the absorption band at about 400-480 cm^{-1}. Three peaks at 3436, 1630 and 1413 cm^{-1} are observed to be in relation to the adsorbed water on the zinc oxide hollow spheres. The wide band at 3436 cm^{-1} is mostly the O–H stretching vibration mode, whereas the peak at 1630 cm^{-1} is the O–H bending band [28, 29]. Consequently, in the presence of the photo-catalyst, only pure ZnO phase were formed – as revealed by both the PXRD and FT-IR analyses of the zinc oxide hollow spheres.
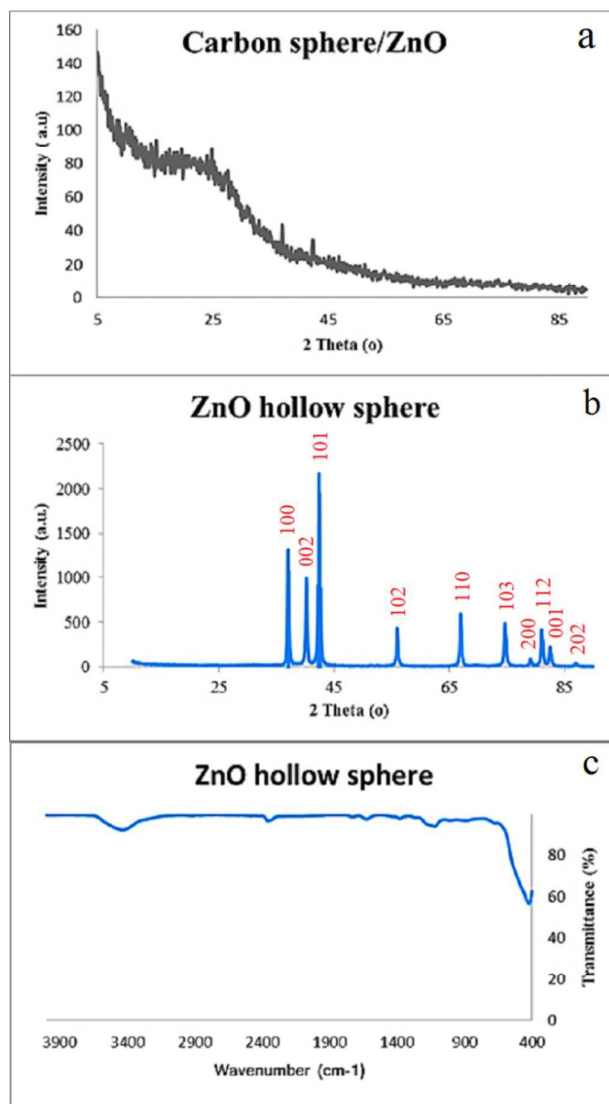
Fig. 4 PXRD diffraction patterns for spherical nanostructures of carbon sphere@ZnO (core/shell) before calcination (a), hollow spherical nanostructures of the ZnO (b), and FT-IR spectra of the ZnO hollow spherical nanostructures (c).

Study of the photocatalytic behavior

Contact time. In this study, degradation of the CR dye – a typical azo dye with two azo bonds (-N=N-) – has been considered as a contamination model from aqueous solution under UV and visible light irradiations in order to estimate the photocatalytic activity of the calcinated ZnO hollow spheres. In order to examine the efficiency of the catalyst for the photocatalytic removal of the said pollutant, CR dye has been applied. The removal efficiency can thus be expressed as follows.

$$Removal\ efficiency = \frac{C_0 - C_t}{C_0} \times 100\% \qquad (1)$$

In the above relation, the initial concentration of the pollutant is signified by C_0 while pollutant concentration in the various irradiation times is shown by C_t. Based on the calculation of the maximum absorption at the wavelength of 315 nm, C_0 and C_t values have been found. In order to control the variations in the CR dye photocatalytic degradation under UV and visible light irradiations,

the UV-Vis spectroscopy has been applied.

Before optimization of the photo-catalytic reaction conditions by the ZnO hollow spheres, a comparison has been made between the different ZnO hollow spheres synthesized under the different heating rates (i.e., 1 ℃ min^{-1}, 2 ℃ min^{-1}, 4 ℃ min^{-1}) to investigate their related photo-catalytic activities for the degradation of the CR dye under both UV and visible light. When the photocatalytic behaviour of these nanostructures was investigated under visible light, much better results were obtained for the prepared hollow spheres with the heating rate of 1 ℃ min^{-1}. As shown in Fig. 5, after the elapsing of 90 min from the start of the reaction time, the photocatalytic activity of the three ZnO nanostructures with the heating rates of 1 ℃ min^{-1}, 2 ℃ min^{-1}, and 4 ℃ min^{-1} were 99.2%, 69%, and 51%, respectively.
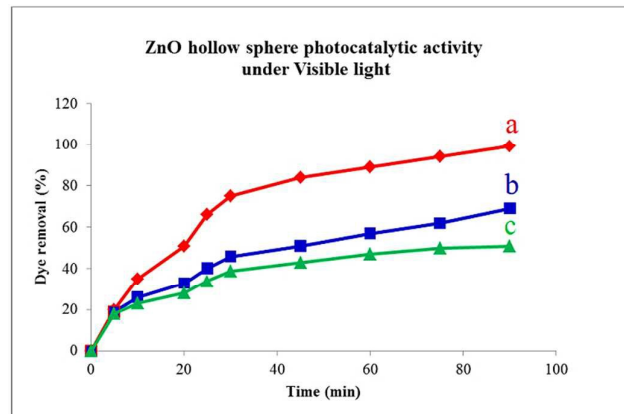
Fig. 5 Photocatalytic efficiency of the CR dye degradation percentage curves by ZnO hollow spheres obtained by calcination at 500 ℃ at the heating rate of 1 ℃ min^{-1} (a), 2 ℃ min^{-1} (b), and 4 ℃ min^{-1} (c) under visible light.

Besides, as shown in Fig. 6, when the said experiment was run for the said three nanostructures under the visible light, after the passing of 45 min from the start of the reaction time, the photocatalytic degradation for the ZnO hollow spheres with the heating rate of 1 ℃ min^{-1} was close to 99%. On the other hand, for two other nanostructures (i.e., ZnO hollow spheres) with the heating rates of 2 ℃ min^{-1} and 4 ℃ min^{-1} after 90 min are 85% and 67%, respectively. This indicates the important role played by the thoroughly synthesized hollow spheres. After the completion of the process and optimization of the reaction conditions, this behaviour is explained in detail. Moreover, through the present study, the prepared hollow spheres with the heating rate of 1 ℃ min^{-1} are henceforth used for the optimization of the aforesaid photocatalyst.
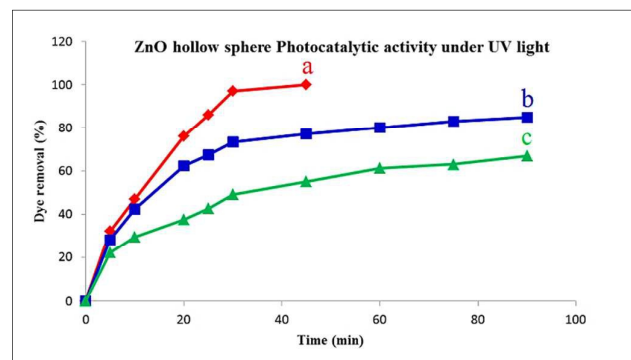
Fig. 6 Photocatalytic efficiency of the CR dye degradation percentage curves by ZnO hollow spheres obtained by calcination at 500 ℃ at the heating rate of 1 ℃ min^{-1} (a), 2 ℃ min^{-1} (b), and 4 ℃
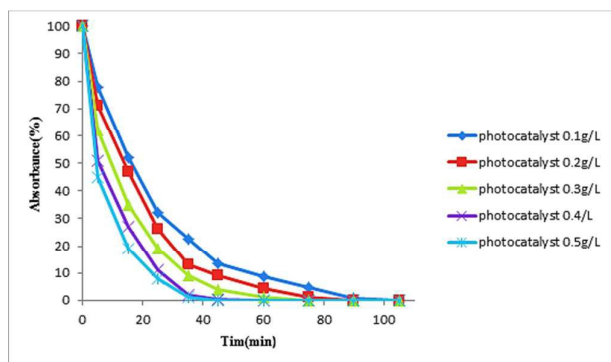
min^{-1} (c) under uv light.

Dependence of the CR dye degradation in the presence and absence of the catalyst under light irradiation is illustrated by Fig. 7. As indicated by Fig. 7a, in the absence of a photocatalyst under UV and visible light irradiation, the CR dye degradation has not been observed. However, as shown in Fig. 7b, after the conduction of the photocatalytic reaction in the dark, a decrease of about 20% occurs in the partial value of the CR dye concentration, which can be called partial adsorption of the organic molecules on the photo-catalytic particle surfaces. The said adsorption value is removed during the photocatalitic activity. Moreover, as illustrated by Figs. 7c and d, in the presence of ZnO hollow spheres under UV and visible light illumination, the percentage of the CR dye degradation increases and closely approaches 99 %.
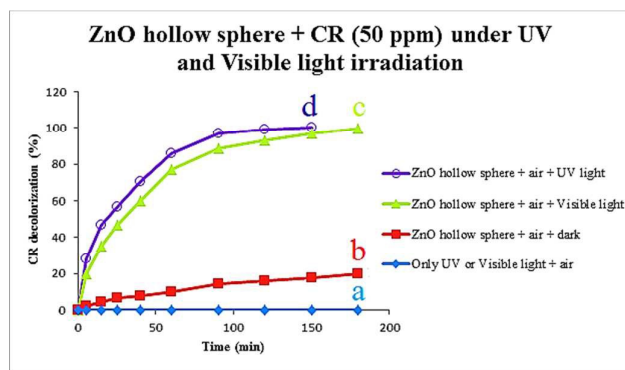
Fig. 7 Photocatalytic efficiency of the CR dye degradation percentage curves: only simulated UV or Visible light (a), ZnO hollow sphere photocatalyst (0.5 gL^{-1}) in dark (b), ZnO hollow sphere photocatalyst (0.5 g L^{-1}) under simulated visible light irradiation (c), and ZnO hollow sphere photocatalyst (0.5 g L^{-1}) under simulated UV light irradiation (d).

The optimum amount of photocatalyst. A crucial factor that determines the photocatalytic efficiency is the catalyst content – in addition to the photocatalyst preparation method. For calculation of the optimal photocatalytic amount, it is required to perform a series reaction at the solutions with different amounts of the zinc oxide hollow spherical structures. Through the change from 0.1 gL^{-1} to 0.5 gL^{-1}, effect of the amount of the photocatalyst on CR compound decolorization has been investigated. Fig. 8 represents the effect of the catalyst amount on the degradation rate. According to this figure, as the catalyst amount increases at the range from 0.1 gL^{-1} to 0.5 gL^{-1}, the kapp values decrease from 60 min to 35 min. This can be accounted for by the fact that the increased catalytic amount results in the increase in the number of the adsorbed photons as well as the increase in the number of the adsorbed dye molecules. Further increases in the catalyst amounts up to 0.5 g L^{-1} result in the slow increases in the kapp values up to 60 min. Therefore, it can be stated that higher catalytic amounts bring about a slight positive effect on the CR dye degradation, which can be ascribed to the accessibility of the active sites on the surface of the catalyst, light scattering, and screening effect [30].

Fig. 8 Effects of amount of the ZnO hallow spheres (0.1-0.5gL^{-1}) on the absorbance of 20 mgL^{-1} CR dye solution under UV light.

The Effect of PH values on the decolorization of CR dye. The catalyst surface property, the ionization state of the organic compound, and the formation rate of hydroxyl radicals and other reactive oxygen species responsible for the pollutant degradation can be changed due to the alteration in PH. Consequently, PH of the solution is another important factor that affects the photodegradation of the organic pollutants. In this regard, all other experimental conditions have been kept constant and the initial PH values of CR dye have been changed from 5 to 9 so that the PH effect on the photocatalytic degradation rate can be investigated. The related results are shown in Fig. 9. Based on the literature, two key factors affecting the pohotocatalyst degradation of the organic pollutants are the production of such active species as OH$^{\bullet}$, O$_2^{\bullet-}$ and hole (h^{+}) and reduction in the e^{-}/h^{+} recombination rate [31]. Fig. 9 also shows that the alkaline solutions have a higher efficiency than the acidic solutions. This result reveals the significant role of the structure and surface properties of the zinc oxide hollow sphere. In other words, the surface charge of the photocatalysts and the potentials of the catalytic reactions might change due to the variations in the solution PH. The positively-charged surface that cannot produce the hydroxyl groups for the formation of the hydroxyl radical is presumed to be in proportion to the low PH. Besides, in order to react with the holes from hydroxyl radicals, higher concentrations of the hydroxyl ions are produced by the higher PH values [32]. However, when the PH value is so high (pH > 8), the dye degradation is inhibited. This can be explained by the fact that the hydroxyl ions compete with the dye molecules in adsorption on the photocatalyst surface. Therefore, at low PH, a reduction in the cationic dyes adsorption on the photocatalytic surface is observed, which is due to the positively-changed photocatalytic surfaces. Besides, due to decreased adsorption, the repulsive forces are observed. As a result, in acidic PH, the efficiency of the degradation decreases, and hence the dye adsorption on the surfaces and subsequently the reaction rates change. In this view, our results demonstrate that UV-Vis absorption spectra is not influenced by the freshly prepared aqueous CR dye solution in PH's including neutral and basic; that is, no aggregation occurs while a change in CR dye decolorization under UV and visible light illumination in aqueous solution at different PH's is observed. It can thus be suggested that, based on our conducted experiments, PH of the reaction solution affects the efficiency of photocatalytic processes. According to the literature, the amphoteric behavior of most semiconductor oxides is a main factor affecting the rate of the reaction occurred on the semiconductor surface. The different behavior of each semiconductor with respect to the PH can normally be explained by the dissimilar modifications of their surface characteristics, which is mostly due to the isoelectrical point (PH ≈ 9.0 for ZnO) [33, 34]. Consequently, at low or high zero point charge (zpc), the surface of the semiconductor is positively or negatively charged, respectively. This behavior can be mainly due to

the effect of the dyes adsorption on the catalyst, which in turn affects the total photocatalytic procedure. In lower zero point charge, the photocatalytic activity of the anionic dyes (primarily sulfonated dyes) such as CR reaches a maximum value. The surface is negatively charged and repels R-SO$_3^{-}$ ions at pH > zpc [35, 36]. Thus, the results demonstrate that PH is one of the determining factors in the dye degradation. Moreover, the optimum PH has been obtained to be about 9.
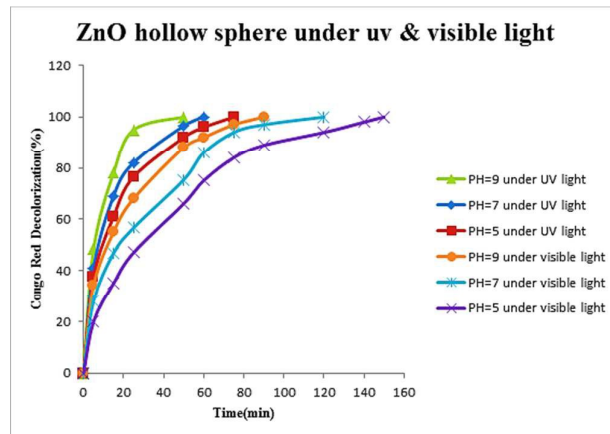

Fig. 9 The Effect of PH values on the decolorization of CR dye (20 ppm) under UV and Visible light irradiation at PH=5 to 9.

The effect of morphology. As recorded in the related literature, the shape and the size of the nanoparticles determine the photocatalytic efficiency of ZnO nanostructures [37]. However, the effects of the morphology of ZnO nanostructure on its photocatalytic behaviors are not yet defined [15]. In this regard, in the next step, through the conduction of some photocatalytic experiments on the degradation of the CR dye, the role of morphology has been taken into account. To this end, and for the investigation and comparison of the photocatalytic activities of the ZnO nanostructures with different morphologies, four other morphologies (rather than the ZnO hollow spheres) have been used. These nanostructures involve the flower like, rod like, rod-flower like, and particle nanostructures (Fig. 10).
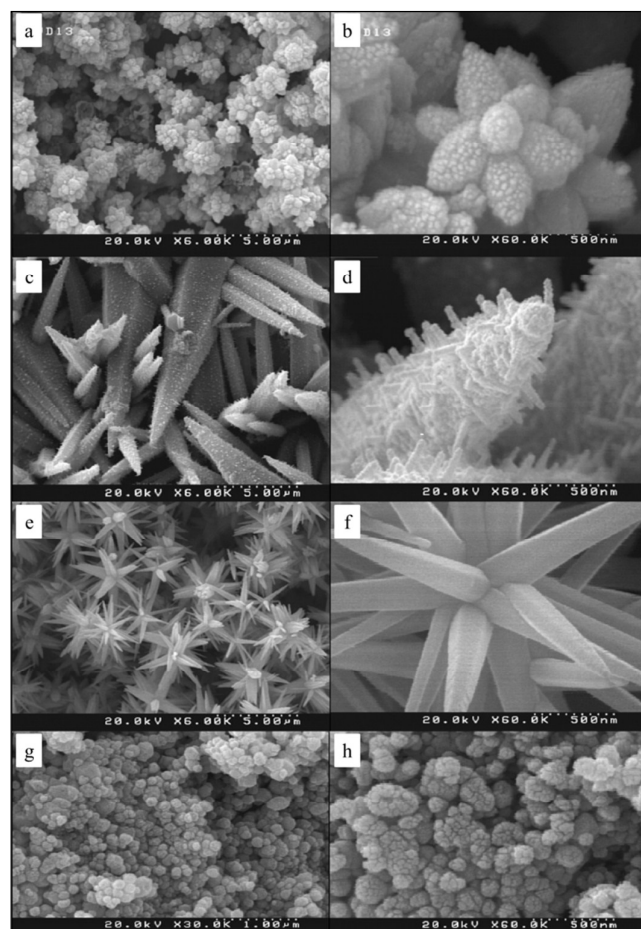
Fig. 10 FE-SEM images of zinc oxide nanostructures synthesized via microwave (a, b), hydrothermal (c, d), solvothermal (e, f), and sol-gel (g, h).

Through the study and comparison of the photocatalytic activities of these nanostructures with those of the ZnO hollow spherical nanostructures, it has been observed that these nanostructures do not provide any promising results under both UV and visible light, even in the case where a longer reaction time (180 min) is involved (Figs. 11 and 12). As these figures show, under visible illumination, the efficiency is 80%, 65%, 57%, and 51% after 180 min for the rod like, flower like, rod-flower like, and particle morphologies, respectively (Fig.11).
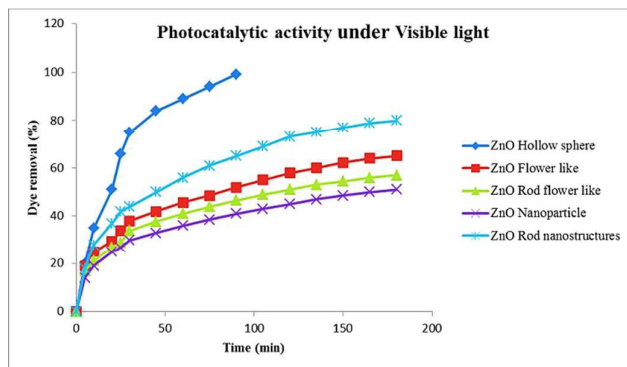

Fig. 11 Photocatalytic efficiency of the CR dye degradation percentage curves by ZnO nanostructures under visible light with different morphologies.

Besides, After 180 min exposure to the UV light irradiation, the efficiency is observed to be 86%, 71.5%, 62%, and 54% for the rod like, flower like, rod-flower like, and particle morphologies, respectively (Fig.12).
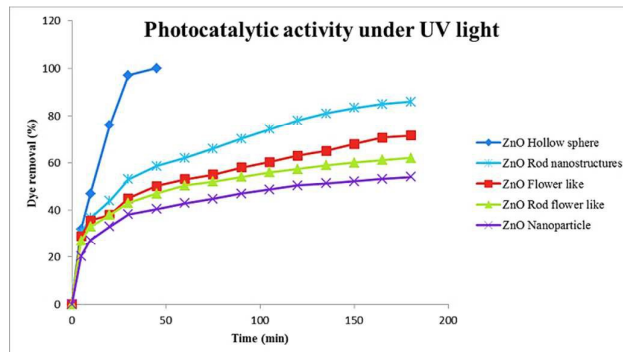
Fig. 12 Photocatalytic efficiency of the CR dye degradation percentage curves by ZnO nanostructures under UV light with different morphologies.

However, as mentioned earlier, complete degradation happens in 45 min under ultraviolet light and 90 min under visible light through the application of the zinc oxide hollow spherical nanostructures obtained from the heating rate of 1 ℃ min^{-1}, at the upper concentration of dye up to 20 ppm (Fig. 13). Moreover, upper destruction times to 45 min are resulted due to the application of the broken ZnO hollow spheres prepared by calcination in upper heating rates of 2 and 4 ℃ min^{-1}. As recorded in the literature, under the irradiation of the ZnO hollow spheres surfaces, some photons enter the porous structure [38]. Microspheres directly adsorb several of these photons while a number of photons are reflected by the spheres. However, only a few numbers of these photons are reflected from the ZnO hollow spheres. On the other hand, most photons remain within the hollow structure until they are totally absorbed. In other words, photon application efficiency can be enhanced by porosity; that is, the porosity enhances the photo-catalytic efficiency. In this context, our synthesized ZnO hollow spheres are expected to demonstrate further advantageous physical characteristics vis-à-vis their potential uses.
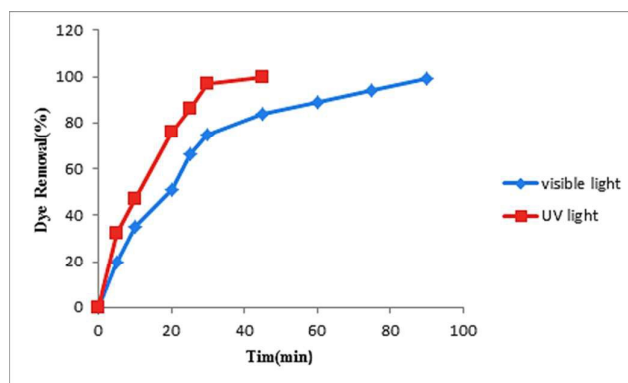
Fig. 13. The photocatalytic performance ZnO hollow spheres for the degradation of CR dye under UV and Visible light irradiation.

Under the hydrothermal conditions, fructose can easily be dehydrated, and subsequently carbon microspheres are formed. The

mechanism for single hollow spheres formation using carbon-precursor based templates has been studied [39]. In this mechanism, carbon microspheres are generally formed as the cores through polymerization and carbonization reaction in the first step of the reaction and hence the dehydration of hydrolyzed metal hydrates in a way that the shells on the hydrophilic carbon cores can be formed. In this regard, the general mechanism of the ZnO hollow spheres formation can also be subdivided into five distinct steps as follows. As recorded in the literature, in the first step, primary carbonaceous spheres are formed due to the dehydration, polymerization, as well as the carbonization of carbon-precursor under hydrothermal conditions [40]. Moreover, it is widely recognized that the spheres have hydrophilic surface that involves considerable -OH and C=O groups due to non-or just partially dehydrated carbon-precursor [41]. Moreover, in order to gradually bind the metal cations through coordination or electrostatic interactions, the hydrophilic groups on the surfaces of the newly formed carbonaceous primary spheres can serve as the "nuclei sites." Resultantly, carbonaceous spheres as cores and a shell of $Zn(OH)_2$ are formed on the external wall of the carbon spheres (step II). In step III, further reaction might also occur between the $Zn(OH)_2$ shell formed on the carbonaceous spheres surface with the -OH groups formed through the dehydration and polymerization of the other residual carbon-precursor, which creates the secondary carbon shell outside the $Zn(OH)_2$ layers. As the hydrolysis of metal salt continues, some extra metal source is provided to form the outer shell (step IV) upon further condensation of $Zn(OH)_2$ species. This results in the creation of the Zn–carbon composites in the hydrothermal treatment process. Ultimately, by the removal of carbon cores, and densification and crosslink of incorporating metal cationic ions in the layer through the calcination, the ZnO hollow spheres are produced (step V). Besides, according to the literature, the size of the hollow spheres is controllable by varying such experimental parameters as the concentration of the initial substances and calcination temperature [42, 43].

Conclusion

Using fast straightforward chemical routes, the present study has sought to synthesize zinc oxide nanostructures with five different morphologies (with flower like, rod like, rod-flower like, particle, and hollow sphere morphologies) so that the effect of morphology in the CR dye degradation can be investigated. Using a novel eco-friendly chemical approach, preparation of the photocatalysts of the nanostructured ZnO hollow spheres (as the best morphology in the CR dye degradation) have been done while carbon spheres have been used as template at the ambience temperature. Using FE-SEM, PXRD, FT-IR, and UV-Visible spectroscopy, the physical and photophysical characteristics of this nanostructure, with morphology of perfectly hollow spheres was characterized. Furthermore, through the application of the HRTEM images, the hollow structure with a bright-colored center cavity and dark-colored shell is clearly seen. In the ZnO lattice, slight or no structural disorder happens – as demonstrated by the PXRD patterns and FTIR spectra. Through the degradation of CR dye, the ZnO hollow spheres photocatalytic activities are investigated. Based on our obtained results, different parameters such as catalyst amount, PH, and shape of the ZnO might affect the rate of degradation. As the photocatalyst amount increases and reaches a plateau at a level of 0.5 g L^{-1}, the degradation rate goes up. Besides, it has been observed that, under both UV and visible light irradiations, the ZnO hollow spheres outperform the other ZnO morphologies in terms of the amount of the photocatalytic activity. Finally, under the assumption that carbon spheres take a key role in the formation of the wurtzite hollow ZnO microspheres, a possible growth mechanism for the ZnO hollow spheres formation has thus been proposed. As a result, the hollow forms of ZnO nanostructures might exert a desired effect on the future industrial and commercial applications, and especially on the photocatalytic degradation of the other organic pollutants.

Acknowledgements

Notes and references

1 W. Wang, M. O. Tadé and Z. Shao, Research progress of perovskite materials in photocatalysis- and photovoltaics-related energy conversion and environmental treatment, *Chem. Soc. Rev.,* 2015, **44**, 5371–5408.
2 R. Asahi, T. Morikawa, H. Irie, and T. Ohwaki, nitrogen-doped titanium dioxide as visible-light-sensitive photocatalyst: designs, developments, and prospects, *Chem. Rev.*, **114**, 2014, 9824–9852.
3 X. Ren, P. Ying, Z. Yang, M. Shang, H. Hou and F. Gao, Foaming-assisted electrospinning of large-pore mesoporous ZnO nanofibers with tailored structures and enhanced photocatalytic activity, *RSC Adv.*, 2015, **5**, 16361–16367.
4 R. Abazari, A. R. Mahjoub and S. Sanati, A facile and efficient preparation of anatase titania nanoparticles in micelle nanoreactors: morphology, structure, and their high photocatalytic activity under UV light illumination, *RSC Adv.*, 2014, **4**, 56406–56414.
5 L. Zhang, Z. Gao, C. Liu, L. Ren, Z. Tu, R. Liu, F. Yang, Y. Zhang, Z. Ye, Y. Li and L. Cui, N-doped nanoporous graphene decorated three-dimensional CuO nanowire network and its application to photocatalytic degradation of dyes, *RSC Adv.*, 2014, **4**, 47455–47460.
6 F. Fazlali, A. R Mahjoub and R. Abazari, A new route for synthesis of spherical NiO nanoparticles via emulsion nano-reactors with Enhanced Photocatalytic Activity, *Solid State Sci.*, 2015, 48, 263–269.
7 K. Jothivenkatachalam, S. Prabhu, A. Nithya and K. Jeganathan, Facile synthesis of WO_3 with reduced particle size on zeolite and enhanced photocatalytic activity, *RSC Adv.*, 2014, **4**, 21221–21229.
8 Y. Hu, D. Li, F. Sun, H. Wang, Y. Weng, W. Xiong and Y. Shao, One-pot template-free synthesis of heterophase $BiVO_4$ microspheres with enhanced photocatalytic activity, *RSC Adv.*, 2015, **5**, 54882–54889.
9 K. Wang, W. Yao, F. Teng and Y. Zhu, Photocatalytic activity enhancement of $LaPO_4$ via surface oxygen vacancies, *RSC Adv.*, 2015, **5**, 56711–56716.
10 D. Li, Y. Zhang, W. Wu and C. Pan, Preparation of a ZnO/TiO_2 vertical-nanoneedle-on-film heterojunction and its photocatalytic properties, *RSC Adv.*, 2014, **4**, 18186–18192.
11 J. Xie, H. Wang, M. Duan and L. Zhang, Synthesis and photocatalysis properties of ZnO structures with different morphologies via hydrothermal method, *Appl. Surf. Sci.*, 2011, **257**, 6358–6363.
12 E. Pelizzetti, C. Minero, P. Piccinini and M. Vincenti, Phototransformations of nitrogen containing organic compounds over irradiated semiconductor metal oxides: Nitrobenzene and Atrazine over TiO_2 and ZnO, *Coord. Chem. Rev.*, 1993, **125**, 183–193.
13 L.-Y. Yang, S.-Y. Dong, J.-H. Sun, J.-L. Feng, Q.-H. Wu and S.-P. Sun, Microwave-assisted preparation, characterization and photocatalytic properties of a dumbbell-shaped ZnO photocatalyst, *J. Hazard. Mater.*, 2010, **179**, 438–443.
14 Y.-C. Chang, ZnO nanopinecone arrays with enhanced photocatalytic performance in sunlight, *RSC Adv.*, 2014, **4**, 20273–20280.
15 N. M. Flores, U. Pal, R. Galeazzi and A. Sandoval, Effects of morphology, surface area, and defect content on the photocatalytic dye degradation performance of ZnO nanostructures, *RSC Adv.*,

2014, **4**, 41099–41110.

16 A. Kołodziejczak-Radzimska and T. Jesionowski, Zinc Oxide-From Synthesis to Application: A Review, *Mater.*, 2014, **7**, 2833–2881.

17 J. Hu, M. Chen, X. Fang and L. Wu, Fabrication and application of inorganic hollow spheres, *Chem. Soc. Rev.*, 2011, **40**, 5472–5491.

18 Y. Yang, Y. Chu, Y. P. Zhang, F. Y. Yang and J. L. Liu, Polystyrene-ZnO core-shell microspheres and hollow ZnO structures synthesized with the sulfonated polystyrene templates, *J. Solid State Chem.*, 2006, **179**, 470–475.

19 P. Bai, P. P. Wu, Z. F. Yan, J. K. Zhou and X. S. Zhao, Self-Assembly of Clewlike ZnO Superstructures in the Presence of Copolymer, *J. Phys. Chem. C*, 2007, **111**, 9729–9733.

20 Z.-Y. Jiang, Z.-X. Xie, X.-H. Zhang, S.-C. Lin, T. Xu, S.-Y. Xie, R.-B. Huang and L.-S. Zheng, Synthesis of Single-Crystalline ZnO Polyhedral Submicrometer-Sized Hollow Beads Using Laser-Assisted Growth with Ethanol Droplets as Soft Templates, *Adv. Mater.*, 2004, **16**, 904–907.

21 X. Jia, H. Fan, F. Zhang and L. Qin, Using sonochemistry for the fabrication of hollow ZnO microspheres, *Ultrason. Sonochem.*, 2010, **17**, 284–287.

22 M. Zhang, H. Yang, Y. Liu, X. Sun, D. Zhang and D. Xue, Hydrophobic precipitation of carbonaceous spheres from fructose by a hydrothermal process, *Carbon*, 2012, **50**, 2155–2161.

23 F. Heshmatpour and R. Abazari, Formation of dispersed palladium–nickel bimetallic nanoparticles in microemulsions: synthesis, characterization, and their use as efficient heterogeneous recyclable catalysts for the amination reactions of aryl chlorides under mild conditions, *RSC Adv.*, 2014, **4**, 55815–55826.

24 R. Abazari and S. Sanati, Room temperature synthesis of tungsten (VI) tri-oxide nanoparticles with one-pot multi-component reaction in emulsion nanoreactors stabilized by aerosol-OT, *Mater. Lett.*, 2013, **107**, 329–332.

25 S. Girish Kumar and K. S. R. Koteswara Rao, Zinc oxide based photocatalysis: tailoring surface-bulk structure and related interfacial charge carrier dynamics for better environmental applications, *RSC Adv.*, 2015, **5**, 3306–3351.

26 M. A. Fox and M. T. Dulay, Heterogeneous photocatalysis, *Chem. Rev.*, 1997, **93**, 341–357.

27 M. Zhang, H. Yang, Y. Liu, X. Sun, D. Zhang and D. Xue, First identification of primary nanoparticles in the aggregation of HMF, *Nanoscale Res. Lett.*, 2012, **7**, 1–13.

28 S. G. Hosseini and R. Abazari, A facile one-step route for production of CuO, NiO, and CuO–NiO nanoparticles and comparison of their catalytic activity for ammonium perchlorate decomposition, *RSC Adv.*, 2015, **5**, 96777–96784.

29 R. Abazari, A. R. Mahjoub, L. A. Saghatforoush and S. Sanati, Characterization and optical properties of spherical WO$_3$ nanoparticles synthesized via the reverse microemulsion process and their photocatalytic behavior, *Mater. Lett.*, 2014, **133**, 208–211.

30 B. Mandal and A. Mondal, Solar light sensitive samarium-doped ceria photocatalysts: microwave synthesis, characterization and photodegradation of Acid Orange 7 at atmospheric conditions and in the absence of any oxidizing agents, *RSC Adv.*, 2015, **5**, 43081–43091.

31 V. J. Babu, S. Vempati and S. Ramakrishna, Reduced recombination and enhanced UV-assisted photocatalysis by highly anisotropic titanates from electrospun TiO$_2$–SiO$_2$ nanostructures, *RSC Adv.*, 2014, **4**, 27979–27987.

32 A. Ajmal, I. Majeed, R. N. Malik, H. Idriss and M. A. Nadeem, Principles and mechanisms of photocatalytic dye degradation on TiO$_2$ based photocatalysts: a comparative overview, *RSC Adv.*, 2014, **4**, 37003–37026.

33 C. Zhu, B. Lu, Q. Su, E. Xie and W. Lan, A simple method for the preparation of hollow ZnO nanospheres for use as a high performance photocatalyst, *Nanoscale*, 2012, **4**, 3060–3064.

34 S. Erdemoğlu, S. Karaaslan Aksu, F. Sayılkan, B. İzgi, M. Asiltürk, H. Sayılkan, F. Frimmel and Ş. Güçer, Photocatalytic degradation of congo red by hydrothermally synthesized nanocrystalline TiO$_2$ and identification of degradation products by LC–MS, *J. Hazard. Mater.*, 2008, **155**, 469–476.

35 M. Huang, C. Xu, Z. Wu, Y. Huang, J. Lin and J. Wu, Photocatalytic decolorization of methyl orange solution by Pt modified TiO$_2$ loaded on natural zeolite, *Dyes Pigm.*, 2008, **77**, 327–334.

36 J. Zhao, T. Wu, K. Oikawa, H. Hidaka and N. Serpone, Photoassisted Degradation of Dye Pollutants. 3. Degradation of the Cationic Dye Rhodamine B in Aqueous Anionic Surfactant/TiO$_2$ Dispersions under Visible Light Irradiation: Evidence for the Need of Substrate Adsorption on TiO$_2$ Particles, *Environ. Sci. Technol.*, 1998, **32**, 2394–2400.

37 K. M. Parida, and S. Parija, Photocatalytic degradation of phenol under solar radiation using microwave irradiated zinc oxide, *Sol. Energy*, 2006, **80**, 1048–1054.

38 H.-Y. Chen, Y.-F. Xu, D.-B.Kuang, and C.-Y. Su, Recent advances in hierarchical macroporous composite structures for photoelectric conversion, *Energy Environ. Sci.*, 2014, **7**, 3887–3901.

39 X. Sun, J. Liu and Y. Li, Use of carbonaceous polysaccharide microspheres as templates for fabricating metal oxide hollow spheres, *Chem. Eur. J.*, 2006, **12**, 2039–2047.

40 X. M. Sun and Y. D. Li, Hollow carbonaceous capsules from glucose solution, *J. Colloid Interface Sci.*, 2005, **291**, 7–12.

41 X. M. Sun, Y. D. Li, Ga$_2$O$_3$/GaN semiconductor hollow spheres, *Angew. Chem. Int. Ed.*, 2004, **43**, 3827–3831.

42 X. Jia, H. Fan, F. Zhang and L. Qin, Using sonochemistry for the fabrication of hollow ZnO microspheres, *Ultrason. Sonochem.*, 2010, **17**, 284–287.

43 L. Zhang, J. Yan, M. Zhou, Y. Yang and Y.-N. Liu, Fabrication and photocatalytic properties of spheres-in-spheres ZnO/ZnAl$_2$O$_4$ composite hollow microspheres, *Appl. Surf. Sci.*, 2013, **268**, 237–245.

Graphical Abstract: